

between the two cases seems to indicate that although 1-butanol is only slightly miscible in water, it is not impossible to imagine that such an interfacial mixture is quite possible if the hydrocarbon chain of the alcohol (and of the SDS) is in the toluene phase, with the hydroxyl in the interfacial layer. Similar behavior of the primary relaxation has been reported by Bertolini et al.<sup>21</sup> for ethanol and 2-propanol solutions with added water. Gestblom and Sjöblom<sup>22</sup> have also observed similar behavior for propanol-water and butanol-water mixtures. The  $\tau_1$  and  $\tau_2$  values given in table 1 of their article<sup>22</sup> for butanol-water mixture within the miscibility limit are very similar to what we observe for the microemulsion composed of water, 1-butanol, SDS, and toluene.

Like Perl et al.,<sup>8</sup> we observe a second relaxation (Figure 11) of nearly constant relaxation frequency of 5 GHz, about a fourth of pure water but equal to that for a secondary relaxation of the neat alcohol. As pointed by Perl et al. there is little doubt about the existence of fast relaxation processes in alcohols in addition to the primary one, but their molecular origins have been a subject of considerable speculation. Mechanisms proposed<sup>8</sup> with numerous variations are changes in hydrogen bonding, either to a new neighbor or within hydrogen-bonded "chains" on the one hand, or to reorientations of unbonded, singly, and multiply bonded

molecular complexes on the other. A more elaborate discussion on the fast relaxation process in alcohol can be found in ref 8.

Finally, it should be recognized that we find the presence of two relaxation processes in all regions of the microemulsion phase. This should give added support to the fact that the relaxation we observe is indeed dipolar. In regions B and C of the microemulsion phase the model of water droplet in oil is no longer valid; we are more in a bicontinuous phase. Any model trying to explain the experimental relaxation as being due to the rotation of the counterions on the micellar surface is certainly not valid in regions B and C of the microemulsion phase. Similarity of the observed relaxation in all three regions of the microemulsion phase lends support to our position of recognizing the relaxation phenomenon as being molecular in origin. Judging from the similarity of the observed relaxation with the relaxation measured in alcohol-water mixture, we therefore conclude that the primary relaxation we observe as being due to water and 1-butanol in the interfacial layer undergoing dipole reorientations with considerable freedom and the experimentally observed fast relaxation process corresponds to the secondary relaxation in 1-butanol.

*Acknowledgment.* This work was supported by the National Sciences and Engineering Research Council of Canada and the Government of Quebec through its FCAR funds.

**Registry No.** SDS, 151-21-3; 1-butanol, 71-36-3; toluene, 108-88-3.

(21) Bertolini, D.; Cassettari, M.; Salvetti, G. *J. Chem. Phys.* **1982**, *76*, 3285.

(22) Gestblom, B.; Sjöblom, J. *Acta Chem. Scand., Ser. A* **1984**, *38*, 575.

## Detergentless Microemulsions as Media for Enzymatic Reactions. Spectroscopic and Ultracentrifugation Studies

Yuri L. Khmelnitsky,\* Arie van Hoek,<sup>†</sup> Cees Veeger, and Antonie J. W. G. Visser

*Department of Biochemistry, Agricultural University, De Dreijen 11, 6703 BC Wageningen, The Netherlands (Received: February 25, 1988; In Final Form: June 28, 1988)*

Analytical ultracentrifugation and time-resolved fluorescence techniques were used to investigate structure and microenvironment of microemulsion droplets existing in ternary systems composed of *n*-hexane, isopropyl alcohol, and water. In fluorescence measurements, rhodamine B was used as a molecular probe sensitive to the environment. Well-defined microdroplets were found only inside a limited area in the triangle phase diagram, their molecular weight and radius being in the range of 3000–5000 daltons and 11–13 Å, respectively. Density and microviscosity of the droplets correspond to those of a water-isopropyl alcohol binary mixture containing approximately 20 vol % of isopropyl alcohol, whereas the micropolarity of droplets interior was close to the polarity of 60–70 vol % solution of isopropyl alcohol in water. The area of existence of well-defined microemulsion droplets in the phase diagram was found to overlap with previously determined locations of maxima of catalytic activity of several enzymes dissolved in *n*-hexane-isopropyl alcohol-water ternary systems. From this observation, the conclusion is drawn that the presence of well-defined microdroplets is a prerequisite for achieving high catalytic activity. Fluorescence anisotropy decay measurements of tryptophan in trypsin dissolved in detergentless microemulsions were used to estimate the size of protein-containing microemulsion droplets. The radius was found to be in the range of 27–37 Å, depending on the composition of the system. The results suggest that at least 10 empty microdroplets are required to produce a droplet large enough to accommodate a protein molecule. On the basis of obtained results, a structural model of protein-containing microemulsion droplets is proposed. According to this model, an enzyme molecule is surrounded by a water-rich layer of 7–10-Å thickness, which serves to protect the enzyme against the denaturing contact with the outer organic phase, thus ensuring the retention of catalytic activity.

### Introduction

Biocatalysis in nonaqueous media has received increasing attention during the last decade. The growing interest in this area of enzymology is accounted for by the advantages in using organic solvents instead of water as a medium for enzymatic reactions. In particular, the replacement of water by organic solvents enables the enzymatic conversion of water-insoluble compounds, the shift

of the equilibrium of enzymatic reactions towards desired products, etc. (for reviews see ref 1). One of the most promising approaches to conduct biocatalytical processes in nonaqueous media has been developed in the framework of micellar enzymology,<sup>2</sup> which deals

\* To whom correspondence should be addressed at A. N. Bach Institute of Biochemistry, USSR Academy of Sciences, 117071 Moscow, USSR.

<sup>†</sup> Permanent address: Department of Molecular Physics, Agricultural University, De Dreijen 11, 6703 BC Wageningen, The Netherlands.

(1) (a) Martinek, K.; Semenov, A. N. *J. Appl. Biochem.* **1981**, *3*, 93. (b) Butler, L. G. *Enzyme Microb. Technol.* **1979**, *1*, 253. (c) Carrea, G. *Trends Biotechnol.* **1984**, *2*, 102. (d) *Biocatalysis in Organic Media*; Laane, C., Tramper, J., Lilly, M. D., Eds.; Elsevier: Amsterdam, 1987. (e) Duarte, J. C. *NATO ASI Ser., Ser. A* **1987**, *128*, 23. (f) Luisi, P. L.; Laane, C. *Trends Biotechnol.* **1986**, *4*, 153. (g) Klibanov, A. M. *Chem. Tech.* **1986**, *6*, 354. (h) Khmelnitsky, Yu. L.; Levashov, A. V.; Klyachko, N. L.; Martinek, K. *Enzyme Microb. Technol.*, in press.

with enzymes or multienzyme systems dissolved in microheterogeneous systems consisting of organic solvent, surfactant, and water. Enzyme molecules in such microemulsion systems are entrapped in aqueous cavities of spherical reversed surfactant micelles and thus become protected against unfavorable contact with the surrounding organic solvent by a layer of water and surfactant molecules.

Recently, we demonstrated<sup>3-5</sup> that so-called detergentless microemulsions formed in ternary systems consisting of a hydrocarbon, isopropyl alcohol (or *n*-propyl alcohol), and water can also be used as a medium for enzymatic reactions. Detergentless microemulsions<sup>6-9</sup> represent thermodynamically stable and optically transparent dispersions of aqueous droplets in a hydrocarbon solvent. The droplets are stabilized by alcohol molecules adsorbed on their surfaces and possess spherical symmetry. Several enzymes, including trypsin,<sup>3</sup> chymotrypsin,<sup>3</sup> laccase,<sup>4</sup> and cholesterol oxidase,<sup>5</sup> have been shown to be active and fairly stable when dissolved in detergentless microemulsions composed of *n*-hexane, isopropyl alcohol, and water.

The literature data concerning the structure and microenvironment of aqueous droplets in detergentless microemulsions are scarce, and nothing is known about the structure of protein-containing microdroplets. Thus, the aim of the present work was to clarify these points by using different physical techniques, such as time-resolved laser fluorescence and analytical ultracentrifugation.

### Experimental Section

**Materials.** Trypsin (grade XI) was obtained from Sigma and used without further purification. Rhodamine B and rose bengal were the products of Eastman Kodak. Rose bengal was additionally purified as described earlier.<sup>10</sup> *p*-Terphenyl was purchased from BDH. Isopropyl alcohol, *n*-hexane, methanol, and ethanol (Merck) were of fluorescent grade. Tris-HCl buffer (0.05 M, pH 8.0) was used as the aqueous component throughout the experiments.

**Preparation of Samples.** Samples for measurements were prepared by simple mixing of required volumes of *n*-hexane, isopropyl alcohol, and water (Tris-HCl buffer) with subsequent vigorous hand-shaking for several seconds until a stable transparent solution was obtained. No further equilibration of samples was needed. Trypsin and rhodamine B were introduced in the form of concentrated stock solutions in Tris-HCl buffer and isopropyl alcohol, respectively.

**Analytical Ultracentrifugation.** Ultracentrifugation experiments were performed by using a MSE Centriscan 75 analytical ultracentrifuge equipped with an optical scanning detection system. For visualization of sedimenting microemulsion droplets they were stained by rhodamine B (overall concentration 3  $\mu$ M); the detection wavelength was 550 nm. Sedimentation velocity and equilibrium runs were carried out at 45 000 and 30 000 rpm, respectively. The data obtained were processed on a Hewlett-Packard 85 microcomputer equipped with a Hewlett-Packard 7470 A plotter. Viscosities were measured by an Ubbelohde viscosimeter (Schott & Gen).

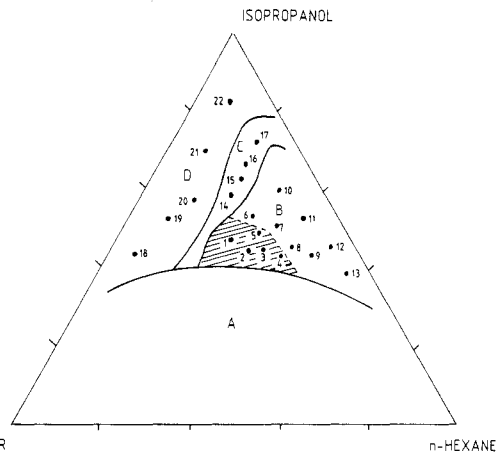


**Figure 1.** Phase diagram of the ternary system *n*-hexane-isopropyl alcohol-water (Tris-HCl buffer, 0.05 M, pH 8.0) at 25 °C.<sup>3</sup> Concentrations of components are given in mole fractions. Numbered points represent compositions studied in this work (see Table I). Structure of phases:<sup>9</sup> A, unstable macroemulsions; B, stable transparent microemulsions; C, H-bonded aggregates of water and isopropyl alcohol dispersed in a hexane-rich medium; D, normal ternary solutions. The dashed area shows the only part of the phase diagram where well-defined microemulsion droplets exist.

**Fluorescence Measurements.** Time-resolved fluorescence experiments were performed as described elsewhere.<sup>11-13</sup> An argon ion laser (Coherent Radiation CR18) was mode-locked, and a rhodamine 6G dye laser (CR 590) was synchronously pumped to yield 580-nm radiation for rhodamine B excitation.<sup>11,14</sup> For a decrease of the 76-MHz repetition rate of the exciting laser pulses to 596 KHz, an electrooptic modulator setup was used.<sup>15</sup> A Balzers B40 598-nm interference filter was combined with a RG590 cutoff filter (Schott) to select rhodamine B fluorescence. For excitation of trypsin at 300 nm a frequency-doubling crystal was used<sup>11</sup> and tryptophan emission was selected with a WG 320 cutoff filter (Schott). A fast 90° rotating sheet polarizer (type HN22 for visible and type HNP'B for ultraviolet) separated the parallel and perpendicular components of fluorescence. The photon detector was a Hamamatsu R 1645U-01 microchannel plate detector. Every 10 s the polarizer was rotated 90° from the original position in 0.3 s, and the different intensity components were stored in two different subgroups of the memory of the multichannel analyzer. Background samples without either rhodamine B or trypsin were recorded under the same conditions. The digital output of the analyzer was transferred to a MicroVAX II computer for data analysis.

Full details of the data analysis including the reference convolution method, weighting schemes, treatment of background, standard errors, and fitting criteria have been given previously.<sup>14,16,17</sup> Use was made of rose bengal in methanol as a reference compound (lifetime 523 ps at 25 °C) for rhodamine B fluorescence and of *p*-terphenyl in ethanol as a reference compound (lifetime 1.06 ns at 25 °C) for tryptophan fluorescence of trypsin. Overall concentration of trypsin was 0.3  $\mu$ M in all cases.

All experiments in this work were carried out at 25 °C.

### Results and Discussion

**Detergentless Microemulsions without Added Protein. Phase Diagram.** The phase diagram of the ternary system *n*-hexane-

(2) (a) Martinek, K.; Levashov, A. V.; Klyachko, N. L.; Khmel'nitsky, Yu. L.; Berezin, I. V. *Eur. J. Biochem.* **1986**, *155*, 453. (b) Luisi, P. L.; Magid, L. J. *CRC Crit. Rev. Biochem.* **1986**, *20*, 409.

(3) (a) Khmel'nitsky, Yu. L.; Zharinova, I. N.; Berezin, I. V.; Levashov, A. V.; Martinek, K. *Dokl. Akad. Nauk SSSR* **1986**, *289*, 1178. (b) Khmel'nitsky, Yu. L.; Zharinova, I. N.; Berezin, I. V.; Levashov, A. V.; Martinek, K. *Ann. N.Y. Acad. Sci.* **1987**, *501*, 161.

(4) Khmel'nitsky, Yu. L.; Gladilin, A. K.; Levashov, A. V.; Martinek, K., manuscript in preparation.

(5) Khmel'nitsky, Yu. L.; Hilhorst, R.; Veeger, C. *Eur. J. Biochem.* **1988**, *176*, 265.

(6) Smith, G. D.; Donelan, C. E.; Barden, R. E. *J. Colloid Interface Sci.* **1977**, *60*, 488.

(7) Keiser, B. A.; Varie, D.; Barden, R. E.; Holt, S. L. *J. Phys. Chem.* **1979**, *83*, 10.

(8) Lund, G.; Holt, S. L. *J. Am. Oil Chem. Soc.* **1980**, *57*, 264.

(9) Smith, G. D.; Barden, R. E. In *Solution Behaviour of Surfactants*; Mittal, K. L., Fendler, E. J., Eds.; Plenum: New York, 1982; Vol. II, p 1225.

(10) Cramer, L. E.; Spears, K. G. *J. Am. Chem. Soc.* **1978**, *100*, 221.

(11) Van Hoek, A.; Vervoort, J.; Visser, A. J. W. G. *J. Biochem. Biophys. Methods* **1983**, *7*, 243.

(12) Van Hoek, A.; Visser, A. J. W. G. *Anal. Instrum. (N.Y.)* **1985**, *14*, 359.

(13) Visser, A. J. W. G.; Ykema, T.; Van Hoek, A.; O'Kane, D. J.; Lee, J. *Biochemistry* **1985**, *24*, 1489.

(14) Visser, A. J. W. G.; Vos, K.; Van Hoek, A.; Santema, J. S. *J. Phys. Chem.* **1988**, *92*, 759.

(15) Van Hoek, A.; Visser, A. J. W. G. *Rev. Sci. Instrum.* **1981**, *42*, 1199.

(16) Vos, K.; Van Hoek, A.; Visser, A. J. W. G. *Eur. J. Biochem.* **1987**, *165*, 55.

(17) Van Hoek, A.; Vos, K.; Visser, A. J. W. G. *IEEE J. Quantum. Electron.* **1987**, *QE-23*, 1812.

**TABLE I: Compositions of Ternary Systems *n*-Hexane–Isopropyl Alcohol–Water Studied in This Work (See Also Figure 1)**

no.	<i>n</i> -hexane		isopropyl alcohol		water (0.05 M Tris–HCl, pH 8)	
	mol fract	vol %	mol fract	vol %	mol fract	vol %
	1	0.265	45.9	0.470	47.8	0.265
2	0.318	52.2	0.440	42.3	0.242	5.5
3	0.356	55.7	0.432	39.7	0.212	4.6
4	0.409	59.0	0.420	37.3	0.171	3.7
5	0.318	50.8	0.477	44.7	0.205	4.5
6	0.288	46.2	0.530	49.8	0.182	4.0
7	0.356	53.4	0.492	43.4	0.152	3.2
8	0.409	58.9	0.455	38.4	0.136	2.7
9	0.470	64.4	0.416	33.4	0.114	2.2
10	0.318	47.2	0.584	50.8	0.098	2.0
11	0.409	56.9	0.508	41.5	0.083	1.6
12	0.497	65.2	0.436	33.6	0.067	1.2
13	0.561	71.1	0.372	27.7	0.067	1.2
14	0.220	37.8	0.568	57.2	0.212	5.0
15	0.205	36.3	0.606	60.0	0.189	3.7
16	0.213	34.1	0.674	63.4	0.112	2.5
17	0.220	34.4	0.697	63.8	0.083	1.8
18	0.061	15.8	0.424	65.3	0.515	18.9
19	0.106	23.4	0.500	64.6	0.394	12.0
20	0.136	27.1	0.553	64.4	0.311	8.5
21	0.106	19.8	0.682	74.7	0.212	5.5
22	0.106	18.1	0.796	79.6	0.098	2.3

isopropyl alcohol–water (Tris–HCl buffer) as determined<sup>3</sup> at 25 °C is shown in Figure 1. According to Smith and Barden<sup>9</sup> the structures of phases in different regions of the phase diagram are as follows. Region A corresponds to unstable opaque macroemulsions that tend to separate rapidly into two phases upon standing. Solutions corresponding to three other realms in the diagram (B–D) are stable and optically transparent. Region D is the area of existence of normal ternary solutions of *n*-hexane, isopropyl alcohol, and water, where no microstructures can be detected. Region B corresponds to microemulsions composed of aqueous microdroplets dispersed in an *n*-hexane-rich outer phase. The existence in region B of a dispersed phase possessing properties of bulk water was confirmed by NMR.<sup>7</sup> Region C is intermediate between regions B and D; in this region H-bonded aggregates of water and isopropyl alcohol dispersed in an *n*-hexane-rich medium are believed to be present.

Numbered points in the phase diagram in Figure 1 represent compositions studied in this work. These are reported in Table I.

**Limits of Occurrence of Microemulsion Droplets.** We found that after prolonged high-speed ( $\geq 45\,000$  rpm) centrifugation of compositions from region B all rhodamine B introduced into the systems could be removed from the solution along with sedimenting microemulsion droplets. This observation implies that rhodamine B exclusively resides inside the droplets and hence can be used to visualize sedimenting boundaries. Clear-cut sedimenting boundaries indicative of the presence of microemulsion droplets were observed only in samples from region B, whereas practically no sedimenting species could be detected in samples from regions D and C. These findings are in full agreement with results obtained by other authors<sup>6</sup> and confirm the existence of microemulsion droplets in region B.

However, the sedimenting behavior of aqueous aggregates was not uniform across region B. Good sedimenting boundaries indicative of the presence of monodisperse droplets were observed only in the lower left corner of region B, where the water content is the highest as compared to other parts of this region. Approximate limits of the area where clear-cut monodisperse aqueous microdroplets exist are shown by the dashed area in Figure 1. On going from this area in any direction toward the *n*-hexane–isopropyl alcohol axis of the phase triangle (i.e., with decreasing water content) sedimenting patterns became increasingly blurred, so that in the vicinity of this axis (e.g., points 10–13 in Figure 1) the shape of sedimenting boundaries indicated the breakdown of mono-

**TABLE II: Characteristics of Microemulsion Droplets from the Dashed Area in Figure 1**

no.	<i>s</i> , S	<i>M</i>	$\rho_d$ , g/cm <sup>3</sup>	<i>r</i> , Å
1	1.06	3200	0.983	10.9
2	1.67	4900	0.993	12.5
3	1.65	4500	0.977	12.3
4	1.82	4800	0.983	12.4
5	1.10	3100	0.978	10.8

disperse aqueous microdroplets into highly polydisperse aggregates.

**Mass and Geometric Characteristics of Microemulsion Droplets.** For compositions inside the dashed area in Figure 1 the results of ultracentrifugation experiments were quantitatively analyzed on the basis of the following assumptions: (1) Aqueous microdroplets are monodisperse spheres. (2) Properties of the outer phase, such as density and viscosity, are identical with those of a binary *n*-hexane–isopropyl alcohol mixture with the same *n*-hexane/isopropyl alcohol volume ratio as in a microemulsion system under consideration.

Data analysis was performed by using well-known expressions,<sup>18</sup> describing the behavior of sedimenting particles, in the following way. The sedimentation coefficient of droplets is given by the Svedberg equation:

$$s = \frac{D}{RT}M(1 - \rho_m/\rho_d) \quad (1)$$

where *R* is the gas constant, *T* is the absolute temperature,  $\rho_m$  is the density of the medium, and *D*, *M* and  $\rho_d$  are the diffusion coefficient, molecular weight, and density of sedimenting droplets, respectively. (In a strict analysis, the value of the sedimentation coefficient should be measured at several concentrations of the dispersed phase and extrapolated to zero concentration, to eliminate the effects of interdroplet interactions. However, such an extrapolation is not possible in the case of the ternary systems under consideration, since one cannot vary the concentration of droplets without influencing their size. For this reason we used a simplified model that assumed the lack of a significant dependence of the sedimentation coefficient on the concentration of droplets. The published data<sup>19,20</sup> show that this assumption is valid at least for some microemulsion systems.) The combination of eq 1 with the Stokes–Einstein equation for the diffusion coefficient of spherical particles gives

$$s = \frac{M}{6\pi\eta r N_A}(1 - \rho_m/\rho_d) \quad (2)$$

where  $N_A$  is the Avogadro number, *r* is the radius of droplets, and  $\eta$  is the viscosity of the medium. The molecular weight of spherical droplets with radius *r* and density  $\rho_d$  is defined by the expression

$$M = \frac{4}{3}\pi r^3 N_A \rho_d \quad (3)$$

On the other hand, the molecular weight of droplets can be extracted from sedimentation equilibrium experiments by using the equation

$$M = \frac{RT(dc/dx)}{(1 - \rho_m/\rho_d)\omega^2 x c} \quad (4)$$

where  $\omega$  is the angular velocity of rotation and *c* is the equilibrium concentration of droplets at a distance *x* from the rotation axis. Processing of experimental data according to eq 4 gives a numerical value *A* defined as

$$A = \frac{M\omega^2}{2RT}(1 - \rho_m/\rho_d) \quad (5)$$

(18) Schachman, H. K. *Ultracentrifugation in Biochemistry*; Academic: New York, 1959.

(19) Robinson, B. H.; Steytler, D. C.; Tack, R. D. *J. Chem. Soc., Faraday Trans. 1* **1979**, *75*, 481.

(20) Candau, F.; Leong, Y. S.; Pouyet, G.; Candau, S. *J. Colloid Interface Sci.* **1984**, *101*, 167.

**TABLE III: Properties of *n*-Hexane-Isopropyl Alcohol and Water-Isopropyl Alcohol Binary Mixtures at 25 °C**

concn of isopropyl alcohol, vol %	<i>n</i> -hexane-iso- propyl alcohol		water-isopropyl alcohol	
	$\rho$ , g/cm <sup>3</sup>	$\eta$ , cP	$\rho$ , g/cm <sup>3</sup>	$\eta$ , cP
0	0.655	0.30	1.00	0.89
20	0.682	0.36	0.981	1.84
40	0.709	0.51	0.952	2.87
60	0.735	0.79	0.901	3.14
80	0.761	1.27	0.848	2.71
100	0.785	2.05	0.785	2.05

Relations 2, 3, and 5 represent a set of three equations with three unknowns, i.e.,  $M$ ,  $\rho_d$ , and  $r$ , which can be found by solving the three equations simultaneously. The values of molecular weight ( $M$ ), radius ( $r$ ), and density ( $\rho_d$ ) of microemulsion droplets existing inside the dashed area in Figure 1 calculated according to the procedure described above are given in Table II together with corresponding sedimentation coefficients. The values of density and viscosity of *n*-hexane-isopropyl alcohol outer phase used in calculations were extracted from the data presented in Table III.

As can be seen from the data in Table II, aqueous droplets existing in detergentless microemulsions composed of *n*-hexane, isopropyl alcohol, and water are quite small (the accuracy of the radius determination is  $\pm 5\%$ ). They are considerably smaller than microdroplets present in toluene-isopropyl alcohol-water microemulsions, whose radii were roughly estimated to be in the range 25–150 Å from light-scattering measurements.<sup>8</sup>

Another important conclusion that can be drawn from the data in Table II relates to the composition of microemulsion droplets. It is most likely that isopropyl alcohol, being highly miscible with water, is partitioned between aqueous microdroplets and *n*-hexane, i.e., droplets should contain a certain concentration of isopropyl alcohol. In other words, droplets may be regarded as tiny fractions of a water-isopropyl alcohol binary mixture dispersed in the *n*-hexane-rich outphase. Hence, the concentration of alcohol present in microemulsion droplets can be estimated by comparing some parameter characterizing the droplets with the same parameter found for bulk water-isopropyl alcohol binary mixtures. One of these parameters is density, which is unambiguously related to the composition of water-alcohol mixtures, as shown in Table III. Comparison of densities  $\rho_d$  of microemulsion droplets taken from Table II with those of water-isopropyl alcohol binary solutions (Table III) shows that the concentration of isopropanol in droplets is about 20% by volume. Simple calculation, based on this result together with the data from Table II, shows that each droplet contains 110–180 molecules of H<sub>2</sub>O and 20–30 molecules of isopropyl alcohol.

**Properties of the Microenvironment inside Microemulsion Droplets.** Rhodamine B, being localized inside microemulsion droplets, represents a very convenient tool for investigation of their interior properties, since the time-resolved fluorescence behavior of this dye is extremely sensitive to its environment.<sup>14</sup> Thus, to get insight into properties of the microenvironment inside microemulsion droplets, such as viscosity and polarity, we performed time-resolved fluorescence and fluorescence anisotropy decay studies of microemulsions using rhodamine B as a probe molecule.

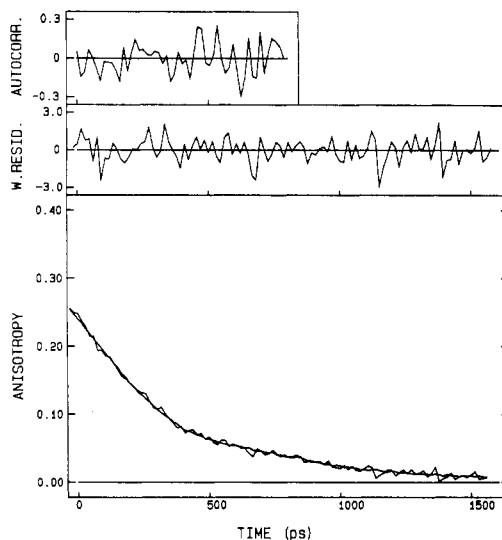


**Figure 2.** Fluorescence anisotropy decay of rhodamine B in detergentless microemulsion (point 3; see Figure 1 and Table I). Only the initial part of the experimental and calculated decay is shown. The quality of the fit is indicated by the weighted residuals and the autocorrelation of these residuals, shown in the upper panels of the plot. Anisotropy parameters are listed in Table IV.

Anisotropy decay data for rhodamine B in all systems studied could be adequately fitted to a monoexponential decay:

$$r(t) = \beta \exp(-t/\phi) \quad (6)$$

where  $\phi$  is the rotational correlation time. As an example, the anisotropy decay curve obtained from a sample corresponding to point 3 (see Figure 1 and Table I) is shown in Figure 2. The values of  $\beta$  and  $\phi$  obtained for compositions from the dashed area in Figure 1 and various water-isopropyl alcohol binary mixtures are given in Tables IV and V, respectively.

The rotational correlation time is related to the rotational diffusion coefficient  $D_{rot}$  of the probe molecule according to the Stokes-Einstein equation

$$\phi = \frac{1}{6D_{rot}} = \frac{4\pi r_0^3 \eta}{3kT} \quad (7)$$

where  $\eta$  is the viscosity,  $k$  is the Boltzmann constant,  $T$  is the absolute temperature, and  $r_0$  is the radius of the effective sphere approximating the probe molecule. The value of  $r_0$  for rhodamine B in water-isopropyl alcohol mixtures calculated by using eq. 7 and values of  $\phi$  and  $\eta$  given in Tables III and V, respectively, was found to equal  $5.50 \pm 0.17$  Å. If we assume, as discussed in preceding sections, that microemulsion droplets are composed of a water-isopropyl alcohol mixture, then this value can be used to calculate microviscosities of droplets from eq 7 on the basis of the values of  $\phi$  given in Table IV. Microviscosities  $\eta_{micro}$  of microemulsion droplets estimated in this way are reported in Table IV. From comparison of these values with viscosities of water-isopropyl alcohol mixtures presented in Table III it can be concluded that the microviscosity in the interior of microemulsion

**TABLE IV: Fluorescent Properties of Rhodamine B in Detergentless Microemulsions and Microviscosity of Microemulsion Droplets**

no.	$\beta$	$\phi$ , ns	$\eta_{micro}$ , cP	$\alpha_1$	$\tau_1$ , ns	$\alpha_2$	$\tau_2$ , ns	$\bar{\tau}_2$ , ns
1	0.348 ± 0.005	0.298 ± 0.004	1.76	0.38 ± 0.10	1.806 ± 0.064	0.62 ± 0.10	2.288 ± 0.037	2.130
2	0.339 ± 0.004	0.294 ± 0.004	1.74	0.47 ± 0.08	1.848 ± 0.038	0.53 ± 0.08	2.220 ± 0.025	2.061
3	0.350 ± 0.004	0.282 ± 0.004	1.67	0.27 ± 0.07	1.708 ± 0.063	0.73 ± 0.07	2.182 ± 0.022	2.075
4	0.351 ± 0.005	0.257 ± 0.004	1.52	0.17 ± 0.03	1.498 ± 0.076	0.83 ± 0.03	2.179 ± 0.014	2.095
5	0.357 ± 0.004	0.255 ± 0.004	1.51	0.20 ± 0.04	1.608 ± 0.061	0.80 ± 0.04	2.211 ± 0.013	2.117
6				0.11 ± 0.01	1.285 ± 0.086	0.89 ± 0.02	2.309 ± 0.008	2.241
7				0.14 ± 0.01	1.308 ± 0.066	0.86 ± 0.01	2.314 ± 0.008	2.230
8				0.14 ± 0.01	1.228 ± 0.065	0.86 ± 0.01	2.283 ± 0.007	2.200
9				0.15 ± 0.02	1.268 ± 0.071	0.85 ± 0.01	2.313 ± 0.010	2.218
10				0.22 ± 0.02	1.444 ± 0.052	0.78 ± 0.02	2.571 ± 0.011	2.420
11				0.22 ± 0.01	1.333 ± 0.042	0.78 ± 0.01	2.545 ± 0.009	2.391
12				0.22 ± 0.01	1.199 ± 0.035	0.78 ± 0.01	2.496 ± 0.007	2.338
13				0.21 ± 0.01	1.132 ± 0.033	0.79 ± 0.01	2.409 ± 0.006	2.265

**TABLE V: Fluorescent Properties of Rhodamine B in Water–Isopropyl Alcohol Binary Mixtures**

concn of isopropyl alcohol, vol %	$\beta$	$\phi$ , ns	$\alpha_1$	$\tau_1$ , ns	$\alpha_2$	$\tau_2$ , ns	$\bar{\tau}_2$ , ns
0	$0.390 \pm 0.008$	$0.167 \pm 0.004$	1.00	$1.558 \pm 0.001$			$1.558^a$
20	$0.371 \pm 0.003$	$0.321 \pm 0.004$	$0.62 \pm 0.08$	$1.850 \pm 0.014$	$0.38 \pm 0.08$	$2.079 \pm 0.032$	1.942
40	$0.372 \pm 0.003$	$0.432 \pm 0.004$	$0.55 \pm 0.10$	$1.878 \pm 0.028$	$0.45 \pm 0.10$	$2.176 \pm 0.036$	2.024
60	$0.365 \pm 0.002$	$0.461 \pm 0.004$	$0.46 \pm 0.09$	$1.894 \pm 0.029$	$0.54 \pm 0.09$	$2.191 \pm 0.027$	2.065
80	$0.364 \pm 0.003$	$0.437 \pm 0.004$	$0.27 \pm 0.05$	$1.852 \pm 0.056$	$0.73 \pm 0.05$	$2.304 \pm 0.013$	2.201
90	$0.360 \pm 0.003$	$0.419 \pm 0.004$	$0.16 \pm 0.04$	$1.720 \pm 0.109$	$0.84 \pm 0.04$	$2.454 \pm 0.018$	2.368
100	$0.342 \pm 0.004$	$0.377 \pm 0.005$	$0.20 \pm 0.03$	$1.878 \pm 0.097$	$0.80 \pm 0.03$	$3.181 \pm 0.021$	3.015

<sup>a</sup>In case of monoexponential decay  $\bar{\tau}_2 = \tau$  (see eq 10).

droplets is approximately 2 times higher than the viscosity of water and corresponds to that found for 15–20% aqueous isopropyl alcohol. This is in good agreement with the composition of droplets estimated from ultracentrifugation measurements.

It should be pointed out that the values of  $\phi$  given in Table IV describe the rotation of the probe inside droplets and not the rotation of droplets as a whole, since in the latter situation the value of  $\phi$ , as estimated from eq 7 by using radii of droplets and viscosity of the outer phase taken from Tables II and III, respectively, would be about 1 ns, which is considerably higher than experimentally observed values (Table IV).

Another useful parameter carrying information about the environment of a fluorophore is the fluorescence lifetime. For rhodamine B dissolved in detergentless microemulsions and in water–isopropyl alcohol binary mixtures the fluorescence decay turned out to be nonexponential and could be fitted with a sum of two-exponential functions:

$$S(t) = \alpha_1 \exp(-t/\tau_1) + \alpha_2 \exp(-t/\tau_2) \quad (8)$$

where  $\tau_1$  and  $\tau_2$  are fluorescence lifetimes, and  $\alpha_1 + \alpha_2 = 1$ . The only exception was rhodamine B dissolved in water, where the fluorescence decay could be adequately described by a monoexponential function. As an example, the fluorescence decay curve obtained in a sample corresponding to point 5 (see Figure 1 and Table I) is shown in Figure 3. The values of  $\alpha_i$  and  $\tau_i$  obtained for compositions from the dashed area in Figure 1 and various water–isopropyl alcohol binary mixtures are given in Tables IV and V, respectively.

The overall decay behavior of a fluorescent probe exhibiting two-exponential decay can be described by the second-order average lifetime defined as

$$\bar{\tau}_2 = \frac{\alpha_1 \tau_1^2 + \alpha_2 \tau_2^2}{\alpha_1 \tau_1 + \alpha_2 \tau_2} \quad (9)$$

As can be seen from Table V, the value of  $\bar{\tau}_2$  is clearly dependent on the concentration of alcohol in water–isopropyl alcohol mixtures and, hence, represents a parameter sensitive to the polarity of the medium in which the fluorophore is embedded. From comparison of  $\bar{\tau}_2$  values found for water–isopropyl alcohol mixtures (Table V) and microemulsion compositions from the dashed area in Figure 1 (Table IV) it can be concluded that the polarity of the microenvironment of rhodamine B incorporated into microemulsion droplets approximately corresponds to that of 60–70% aqueous isopropyl alcohol. This is considerably higher than the estimated 20% concentration of isopropyl alcohol in droplets obtained from ultracentrifugation and fluorescence anisotropy decay experiments. However, this apparent discrepancy can be easily explained if one takes into account that the observed polarity of microemulsion droplets is known<sup>21</sup> to be in many cases much lower than that of the liquid from which the droplets are formed.

Table IV also contains fluorescence decay parameters of rhodamine B determined at the points in region B lying outside the dashed area in Figure 1. Comparison with corresponding values of  $\tau_2$  in binary mixtures clearly indicates that the polarity of the

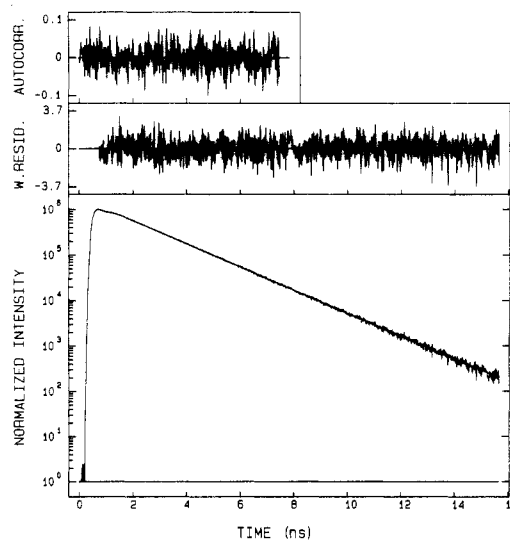


**Figure 3.** Fluorescence intensity decay and fit of rhodamine B in detergentless microemulsion (point 5; see Figure 1 and Table I). Intensity is in arbitrary units. Decay parameters are given in Table IV.

microenvironment of rhodamine B inside microemulsion aggregates steeply decreases on going outside the dashed area. This result can be interpreted in terms of partial breakdown of microemulsion droplets with concomitant increase in isopropyl alcohol concentration in their interior, which is completely in line with the conclusion made from ultracentrifugation experiments (see above).

#### *Detergentless Microemulsions Containing Solubilized Trypsin.*

In our previous studies<sup>3</sup> we have shown that the profile of enzymatic activity of trypsin dissolved in *n*-hexane–isopropyl alcohol–water ternary systems reveals a single sharp maximum falling on the microemulsion region of the phase diagram (region B in Figure 1). The same result also has been obtained for another enzyme, laccase.<sup>4</sup> One of the most important implications of the present study is that the position of the maximum of catalytic activity for both enzymes exactly coincides with the location of the dashed area in Figure 1, the only part of the phase diagram where well-defined microemulsion droplets are found. In other words, the presence of sufficiently large and well-defined microdroplets is a prerequisite for achieving high catalytic activity in the ternary systems under consideration.

To estimate the size of protein-containing microemulsion droplets, we measured the anisotropy decay of tryptophan fluorescence of trypsin dissolved in ternary *n*-hexane–isopropyl alcohol–water systems from region B in Figure 1. In all cases the anisotropy decay turned out to be nonexponential and could be fitted with a sum of two-exponential functions:

$$r(t) = \beta_1 \exp(-t/\phi_1) + \beta_2 \exp(-t/\phi_2) \quad (10)$$

As an example, the anisotropy decay curve obtained from a trypsin-containing sample corresponding to point 1 (see Figure 1 and Table I) is shown in Figure 4. The values of  $\beta_i$  and  $\phi_i$  determined for trypsin dissolved in several compositions from the microemulsion region are presented in Table VI. The short correlation times  $\phi_1$  can be assigned to internal fast movements

(21) (a) Wong, M.; Thomas, J. K.; Gratzel, M. *J. Am. Chem. Soc.* **1976**, *98*, 2391. (b) Zinsli, P. E. *J. Phys. Chem.* **1979**, *83*, 3223.

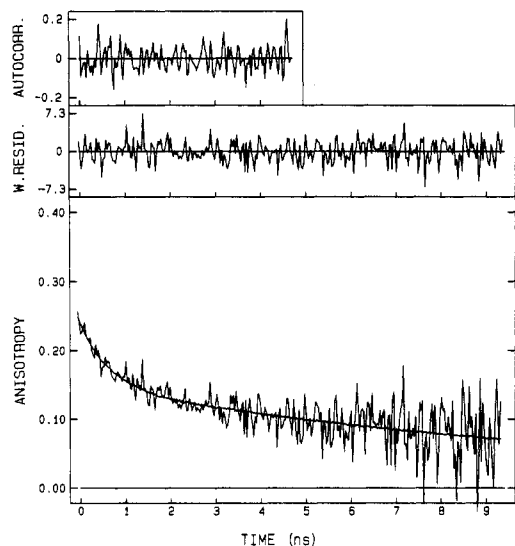


Figure 4. Fluorescence anisotropy decay of trypsin in detergentless microemulsion (point I; see Figure 1 and Table I). Anisotropy parameters are given in Table VI.

TABLE VI: Anisotropy Decay Parameters of Trypsin in Detergentless Microemulsions and Radii of Trypsin-Containing Microemulsion Droplets

no.	$\beta_1^a$	$\phi_1$ , ns	$\beta_2^a$	$\phi_2$ , ns	$r_p$ , Å
1	0.14	$0.58 \pm 0.06$	0.14	$13.3 \pm 1.1$	$27.2 \pm 0.8$
3	0.17	$0.42 \pm 0.07$	0.16	$14.1 \pm 1.2$	$29.5 \pm 0.9$
6	0.12	$0.72 \pm 0.08$	0.14	$15.0 \pm 1.6$	$28.2 \pm 1.1$
7	0.11	$0.85 \pm 0.09$	0.10	$14.4 \pm 1.7$	$29.0 \pm 1.2$
8	0.13	$0.78 \pm 0.08$	0.13	$16.6 \pm 2.0$	$31.7 \pm 1.3$
9	0.12	$0.75 \pm 0.12$	0.12	$14.8 \pm 1.9$	$31.9 \pm 1.5$
10	0.12	$0.65 \pm 0.13$	0.13	$18.1 \pm 1.9$	$30.0 \pm 1.1$
11	0.12	$0.67 \pm 0.08$	0.13	$19.1 \pm 1.7$	$32.4 \pm 1.0$
12	0.15	$0.52 \pm 0.06$	0.16	$22.6 \pm 2.5$	$36.7 \pm 1.4$
13	0.12	$0.56 \pm 0.07$	0.14	$21.2 \pm 2.1$	$37.3 \pm 1.2$

<sup>a</sup>Standard deviation is less than 0.01.

of the part of the polypeptide chain that contains tryptophan residues, whereas much longer correlation times  $\phi_2$  are obviously related to an overall rotation of protein molecules.

Before any further interpretation of the data could be made, it was necessary to establish whether the rotational correlation times  $\phi_2$  (Table VI) described the movement of protein molecules inside droplets or the rotation of protein-containing droplets as a whole. To clarify this point, we studied the fluorescence behavior of trypsin in various water-isopropyl alcohol binary mixtures that mimic the microenvironment inside microemulsion droplets, as discussed in preceding sections. As in microemulsion systems, the anisotropy decay of trypsin fluorescence in binary mixtures also turned out to be biexponential, and corresponding values of  $\beta_1$  and  $\phi_1$  are given in Table VII. Comparison of the data in Table VI and Table VII clearly shows that  $\phi_2$  values found in model water-isopropyl alcohol mixtures are significantly lower than those observed in microemulsions. Hence, we can conclude that rotational correlation times  $\phi_2$  reported in Table VI describe the rotation of protein-containing droplets as a whole and not the movement of trypsin in their interior.

Radii  $r_p$  of protein-containing microemulsion droplets calculated from  $\phi_2$  values for trypsin by using eq 7 are given in Table VI. In these calculations the viscosity of the outer phase was taken equal to that of corresponding *n*-hexane-isopropyl alcohol binary mixtures (Table III), in the same way as it was assumed above in the analysis of ultracentrifugation data. It is clearly seen that droplets containing entrapped protein molecules are considerably larger than their empty counterparts (cf. radii of droplets in protein-free microemulsions reported in Table II). This result is by no means surprising since initial water droplets are much smaller than trypsin molecules, whose hydrodynamic radius in aqueous solution was estimated by using eq 7 to be about 20 Å,

TABLE VII: Anisotropy Decay Parameters of Trypsin in Water-Isopropyl Alcohol Binary Mixtures

concn of isopropyl alcohol, vol %	$\beta_1$	$\phi_1$ , ns	$\beta_2^a$	$\phi_2$ , ns
0	0.12	$0.35 \pm 0.18$	0.12	$6.2 \pm 1.1$
20	0.10	$0.40 \pm 0.21$	0.11	$7.1 \pm 0.8$
40	0.12	$0.47 \pm 0.15$	0.10	$9.4 \pm 1.0$
60	0.13	$0.40 \pm 0.12$	0.12	$9.2 \pm 0.8$
80	0.13	$0.51 \pm 0.12$	0.13	$10.0 \pm 0.9$

<sup>a</sup>Standard deviation is less than 0.01.

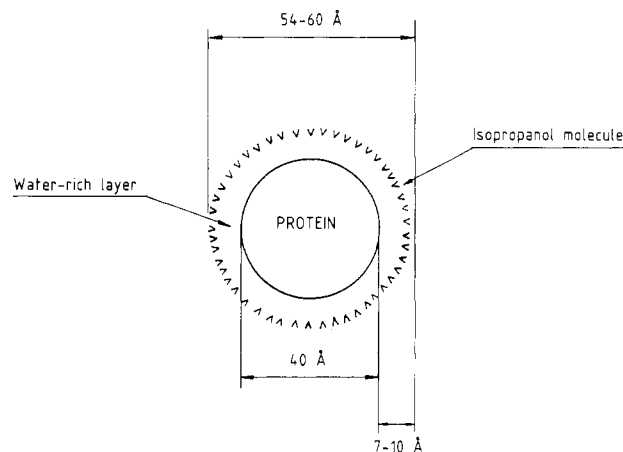


Figure 5. Structural model of protein-containing microemulsion droplets existing in the dashed area in Figure 1.

in good agreement with the literature value.<sup>22</sup> Simple calculations show that at least 10 empty droplets are required to build up a droplet with entrapped trypsin molecule.

On the basis of the above results, a structural model of trypsin-containing microemulsion droplets existing in the dashed area in Figure 1 can be put forward. According to this model, as depicted schematically in Figure 5, the enzyme molecule is surrounded by a water-rich layer (containing presumably about 20% of isopropyl alcohol) of 7–10-Å thickness, which serves to separate the enzyme from unfavorable contact with the organic outer phase. We suggest that it is the existence of this protective layer that makes it possible to retain high catalytic activity of enzymes dissolved in detergentless microemulsions. In main features the structure shown in Figure 5 is very much the same as in the case of conventional, surfactant-based microemulsions containing proteins<sup>23</sup> with the exception that in detergentless microemulsions no surfactant is needed to stabilize the droplets. As to the structure of protein-containing droplets existing in other parts of region B outside the dashed area in Figure 1, it is supposedly similar to that shown in Figure 5, except that the concentration of isopropyl alcohol in the water-alcohol layer surrounding the protein molecule becomes much higher, as one may suggest from results of fluorescence lifetime measurements of rhodamine B in corresponding systems (see above). To put it differently, the layer tends to become denaturing instead of being protective, so that the catalytic activity of enzyme must decrease on leaving the dashed area in Figure 1. The latter trend was indeed observed experimentally.<sup>3</sup>

The results presented in Table VI also imply that the size of protein-containing microemulsion droplets increases on going outside the dashed area in Figure 1. The reason for such behavior remains unclear. One possible explanation, which could be valid at least in some cases, is that denatured protein molecules form aggregates, thus increasing the size of the droplet required for their accommodation. For example, protein-containing droplets

(22) Squire, P. G.; Himmel, M. E. *Arch. Biochem. Biophys.* **1979**, *196*, 165.

(23) Levashov, A. V.; Khmel'nitsky, Yu. L.; Klyachko, N. L.; Chernyak, V. Ya.; Martinek, K. *J. Colloid Interface Sci.* **1982**, *88*, 444.

existing in the system corresponding to point 13 are large enough to accommodate a trypsin dimer (see Table VI).

### Concluding Remarks

Detergentless microemulsions represent a novel promising microheterogeneous medium suitable for carrying out enzymatic reactions under conditions of low and controlled water content. In many respects these unusual systems are similar to ordinary surfactant-based microemulsions: both of them are thermodynamically stable transparent dispersions of aqueous microdroplets in organic solvent capable of solubilizing catalytic amounts of different enzymes with retention of their catalytic activity and stability, and both types of systems provide convenient means to conduct enzymatic conversions of water-insoluble compounds. Moreover, results of the present work show that detergentless microemulsions and proteins dissolved in them can be adequately investigated with the same techniques that are normally used in case of conventional surfactant-based microemulsions. This becomes possible due to the fact that protein-containing detergentless microemulsions are homogeneous and transparent solutions, in contrast to heterogeneous suspensions of solid-state enzymes in

organic solvents used by Klibanov.<sup>18</sup>

However, the great advantage of detergentless microemulsions as compared to conventional microemulsions is that the former do not contain any surfactant. Owing to this fact the problem of separation of reaction products and enzyme regeneration can be solved very easily, quite in contrast with the situation when surfactant-based systems are used. This aspect of practical application of detergentless microemulsions has been demonstrated by us on the example of cholesterol conversion catalyzed by cholesterol oxidase.<sup>5</sup>

*Acknowledgment.* Part of this work was supported by the Netherlands Foundation of Chemical Research (SON) with financial aid from the Netherlands Organization for the Advancement of Pure Research (ZWO). Y.L.K. is grateful to the Agricultural University of Wageningen for awarding a fellowship. We thank A. H. Westphal for help in the ultracentrifugation measurements, J. C. Toppenberg-Fang for the preparation of the manuscript, and M. M. Bouwmans for drawing the figures.

**Registry No.** *n*-Hexane, 110-54-3; isopropyl alcohol, 67-63-0; trypsin, 9002-07-7.

## Intrazeolite Metallocenes: Chemistry, Spectroscopy, and Dynamics

Geoffrey A. Ozin\* and John Godber†

Lash Miller Chemistry Laboratories, University of Toronto, 80 St. George Street, Toronto, Ontario, Canada M5S 1A1 (Received: February 29, 1988; In Final Form: June 17, 1988)

Optical, vibrational, and paramagnetic resonance spectroscopic studies have been conducted on Cp<sub>2</sub>M (M = Cr, Fe, Co) and some of their ring substituted derivatives, impregnated by solution- and gas-phase techniques into a range of ion-exchanged Y and A zeolites, including the Bronsted acid form of Y zeolite. The main focus of the study is directed toward the intrazeolite chemistry, spectroscopy, and dynamics of Cp<sub>2</sub>M/Cp<sub>2</sub>M<sup>+</sup> redox pairs. Key points to emerge from this study relate to the following: (1) kinetics of intrazeolite impregnation/diffusion of Cp<sub>2</sub>M, (2) internal versus external confinement of Cp<sub>2</sub>M/Cp<sub>2</sub>M<sup>+</sup> guests, (3) spacially resolved intrazeolite redox titrations and the homogeneity of a Cp<sub>2</sub>M/Cp<sub>2</sub>M<sup>+</sup> impregnation into the zeolite crystals, (4) intrazeolite redox chemistry in H<sub>n</sub>D<sub>m</sub>Na<sub>56-n-m</sub>-Y isotopically labeled zeolites, and (5)  $\alpha$ -cage Bronsted acid site-specific electron-transfer processes and redox-induced H-atom/lattice OH production of H<sub>2</sub>O, with concurrent production of Cp<sub>2</sub>M<sup>+</sup> with Al<sup>+</sup> and Si<sup>+</sup> framework radical centers (the ratio of the latter being dependent on the concentration of Bronsted acid sites). (6) For orbitally degenerate ground-state Cp<sub>2</sub>Cr and Cp<sub>2</sub>Fe<sup>+</sup>, the intrazeolite anchoring site, g-tensor anisotropy  $\Delta g$ , low symmetry distortion parameter  $\delta$ , and cage dynamics are extremely sensitive to the level of ion exchange, co-cation types, and temperature. (7) This is to be contrasted with orbitally nondegenerate intrazeolite Cp<sub>2</sub>Cr<sup>+</sup>, whose magnetic parameters are rather insensitive to the host matrix. (8) Controlled O<sub>2</sub> oxidation of intrazeolite Cp<sub>2</sub>Cr/Na-Y leads to spacially separated and charge-separated cation/anion pairs, Cp<sub>2</sub>Cr<sup>+</sup>/O<sub>2</sub><sup>-</sup>. (9) Analysis of the hyperfine tensors for framework Al<sup>+</sup> radical centers in Cp<sub>2</sub>M/H<sub>n</sub>Na<sub>56-n</sub>-Y zeolites leads to a hybridization ratio of sp<sup>2.06-2.09</sup> and an almost triangular planar configuration of oxygens about the Al in the AlO<sub>3</sub> site with  $\phi = 119^\circ$ .

### Introduction

Loading organometallic complexes into dehydrated zeolites leads to materials in which the chemical and physical properties of both the "guest" and the "host" are often modified. The internal architecture of zeolites offers a unique environment to adsorbates, which is intimately related to the structure, where essentially every atom is on the "surface", that is accessible to adsorbates.<sup>1</sup> Thus the effects of high internal electric fields,<sup>2</sup> the presence of "coordinatively unsaturated" extraframework cations,<sup>1</sup> and an oxide framework which may contain Bronsted acid, Lewis acid, and Lewis base sites<sup>3</sup> all find their origin in the fact that the zeolite structure and its bonding properties result in what may be thought of as an expanded ionic lattice.<sup>4</sup> The changes induced in a dehydrated zeolite upon molecules entering the internal pores and cavities tend toward the polarization of charge<sup>5</sup> and a lowering of the energy of the guest-host system by attempting to recreate

the charge distribution initially present in the hydrated form.<sup>6</sup> This is the source of their catalytic efficacy.<sup>4</sup> We report here details on the existence and properties of the guest-host system formed from zeolite Y and the well-known metallocenes ferrocene, chromocene, and cobaltocene.<sup>7</sup>

(1) Mortier, W. J.; Schoonheydt, R. A. *Prog. Solid State Chem.* **1985**, *16*, 1, and references cited therein.

(2) Preuss, E.; Linden, G.; Peuckert, M. *J. Phys. Chem.* **1985**, *89*, 2955, and references cited therein.

(3) Barthomeuf, D. *Zeolites: Science and Technology*; NATO ASI Series, Series E: Applied Sciences 80; Martinus Nijhoff: The Hague, 1984; p 317, and references cited therein.

(4) Kasai, P. H.; Bishop, R. J. *Zeolite Chemistry and Catalysis*; ACS Monograph Series 171; American Chemical Society: Washington, DC, 1976; p 350.

(5) Rabo, J. A. *Zeolite Chemistry and Catalysis*; ACS Monograph Series 171; American Chemical Society: Washington, DC, 1976; p 332.

(6) Rabo, J. A. *Proceedings of the VIth International Zeolite Conference*; Olson, D., Bisio, A., Eds.; Butterworth: Guildford, Surrey, U.K., 1984; p 41.

(7) Ozin, G. A.; Godber, J. *ACS Symp. Ser.* **1986**, *307*, 212. Godber, J. Ph.D. Thesis, University of Toronto, 1987.

\* Present address: Albright and Wilson Americas, 2 Gibbs Road, Islington, ON, Canada M9B 1R1.